Bone Pose Estimation in the Presence of Soft Tissue Artifact Using Triangular Cosserat Point Elements

Dana Solav[1], MB Rubin[1], Andrea Cereatti[2,4], Valentina Camomilla[3,4], and Alon Wolf[1]

[1] Department of Mechanical Engineering, Technion Israel Institute of Technology, 32000 Haifa, Israel

[2] POLCOMING Department, Information Engineering Unit, University of Sassari, 07100 Sassari, Italy

[3] Department of Movement, Human and Health Sciences, University of Rome "Foro Italico", 00135 Rome, Italy

[4] Interuniversity Centre of Bioengineering of the Human Neuromusculoskeletal system, University of Rome "Foro Italico", 00135 Rome, Italy

Address correspondence to Dana Solav, Department of Mechanical Engineering, Technion Israel Institute of Technology, 32000 Haifa, Israel. Electronic mail: danas@technion.ac.il.

Submitted to the Annals of Biomedical Engineering, January 2015. Accepted July 2015.

https://doi.org/10.1007/s10439-015-1384-6

ABSTRACT

Accurate estimation of the position and orientation (pose) of a bone from a cluster of skin markers is limited mostly by the relative motion between the bone and the markers, which is known as the Soft Tissue Artifact (STA). This work presents a method, based on continuum mechanics, to describe the kinematics of a cluster affected by STA. The cluster is characterized by Triangular Cosserat Point Elements (TCPEs) defined by all combinations of three markers. The effects of the STA on the TCPEs are quantified using three parameters describing the strain in each TCPE and the relative rotation and translation between TCPEs. The method was evaluated using previously collected *ex-vivo* kinematic data. Femur pose was estimated from 12 skin markers on the thigh, while its reference pose was measured using bone pins. Analysis revealed that instantaneous subsets of TCPEs exist which estimate bone position and orientation more accurately than the Procrustes Superimposition applied to the cluster of all markers. It has been shown that some of these parameters correlate well with femur pose errors, which suggests that they can be used to select, at each instant, subsets of TCPEs leading an improved estimation of the underlying bone pose.

Key Terms: Bone pose estimation; Cosserat point theory; marker cluster; motion analysis; soft tissue artifact; soft tissue deformation; stereophotogrammetry; Triangular Cosserat Point Element.

INTRODUCTION

In human movement analysis, bony segments are generally considered as non-deformable. However, due to the presence of soft tissues surrounding the bone, the related body segments behave as deformable bodies. When non-invasive techniques such as stereophotogrammetry are used, the accurate estimation of the position and orientation (pose) of a rigid bony segment from the measured position of markers attached to the skin is limited mostly by the relative motion between the markers and the bone, which is known as the Soft Tissue Artifact (STA) [26]. In the literature, several methods have been proposed that employ clusters composed of a redundant number of skin markers (>3) and which exploit this redundancy to minimize the effect of the STA on the estimation of the underlying bone pose, but no satisfactory solution yet exists [26, 29].

Since there is no unique separation of the kinematics of a deformable body into rigid and non-rigid motion, any estimation of the rigid motion of the underlying bone pose necessarily depends on non-unique definitions. Nevertheless, attempts have been made to separate the effect of the STA into a rigid motion (RM) of the cluster relative to the bone and non-rigid motion (NRM) of the cluster. Various different representations of these two contributions of the STA have been suggested [2-4, 19, 20, 23]. Most of the studies have shown that the STA’s RM component has a similar [23] or larger magnitude than the STA’s NRM component [2, 4, 5, 19, 21]. Therefore, commonly used techniques that compensate only for cluster NRM [15-17, 25, 32, 37] are insufficient to fully compensate for the STA effects, while the RM component, considered only in few compensation methods [10, 19], has been recently claimed as the only relevant component to be incorporated in pose estimators that can effectively compensate for the STA [21].

The most recent studies show that the RM component represents the main portion of the STA, using different representations for the cluster movement and transformation. Barré et al.[4] assessed the RM component of the STA, during treadmill walking, using the Procrustes Superimposition (PS) approach [11] applied on the entire cluster of markers and showed that it represents approximately 80-100% of the STA amplitude. A similar conclusion was reached in three other works: de Rosario et al. [19] , who defined the NRM and RM components of the STA as the symmetric and skew-symmetric components of the vector field representing the relative marker displacements; Dumas et al. [21], who used the modal approach [20] to split the STA into additive components representing the RM and NRM cluster geometrical transformations in running; and Benoit et al. [5], who modelled the cluster as resizable and deformable and described the STA components for walking, cutting maneuver, and one-legged hops. However, all cited STA quantifications analyze the kinematics of the entire cluster, and do not account for the fact that different sub-clusters within the large cluster of markers may demonstrate different kinematics [22, 23].

Attempts have been made to exploit the different kinematics of multiple sub-clusters to estimate the STA; Camomilla et al. [9] identified a subset of the latter clusters endowed with uncorrelated local movements and used the coherent average of the vectors reconstructed using them to estimate the STA; however, this estimate is affected by a phase indeterminacy that does not allow using the method to compensate for STA. Two studies investigated the possibility of using the NRM component, accessible from non-invasive measurements, to predict the RM components, or the pose errors. Stagni and Fantozzi [35] described the NRM component as the standard deviation of inter-marker pair distances and the RM component of a cluster made of all available markers, as the standard deviation of the cluster center position and of the Euler rotation angle of its principal axes of inertia. Grimpampi et al. [23] defined a new set of metrics for the description of the RM and NRM component, by examining the maximum variation in the time domain of position and orientation range for RM, and of size and shape range, for NRM. However, both studies obtained mostly poor correlations between RM and NRM, and concluded that the selection of clusters allowing for NRM minimization would not entail minimization of the RM component and, therefore, cannot be used for STA compensation. Nevertheless, these results are not conclusive, since both analyses are based upon maximum variations over time, and do not assess the possible instantaneous correlations between the different components.

In a previous work by some of the authors [33], a new approach for the description of the deformation of clusters of skin markers was presented. The cluster of markers was characterized with Triangular Cosserat Point Elements (TCPEs) defined by all combinations of three markers and the kinematics of each TCPE was analysed using the nonlinear continuum mechanics theory of a Cosserat point with homogeneous deformations [30]. The main idea of the TCPE method is to use physical deformation parameters to identify instantaneous subsets of TCPEs which predict the best possible bone pose in the presence of STA. In the previous work, the orientation of a rigid pendulum was estimated from the trajectories of markers fixed to a deformable silicone implant attached to its distal part, as a simulation of soft tissues around a bone. It was shown that partial compensation for the STA can be achieved by selecting subset groups of TCPEs having small strains and small relative rotations between them. However, the relative translations between TCPEs and the estimation of the position of the body were not taken into account.

The current work stems from these premises and both expands the method to characterize relative differences in the translations of TCPEs and further analyzes the ability of the physical deformation parameters to identify characteristics of those instantaneous subsets of TCPEs which most accurately estimate the bone pose.

The original aspects of the current study, including the TCPE developments, are the following:

1. The motion is quantified using physical parameters by analyzing the markers as Lagrangian material points in a continuum, rather than by applying purely mathematical or geometrical approximations.
2. The effects of the STA on sub-clusters of three markers (characterized by TCPEs) are described in terms of the strain in each TCPE and the relative rotation and relative translation between TCPEs.
3. The parameters are instantaneous, allowing for the selection of different subsets at each time step, rather than using a single marker cluster for the entire duration of the trials.

In this work, the developed method is applied to a set of previously collected *ex-vivo* data on the motion of the lower limbs of three cadavers with accurate measurements of the underlying bone pose [14, 23].

MATERIALS AND METHODS

The proposed method determines the pose of a bone segment from markers placed on the skin of the segment. These markers are combined into all possible clusters of three markers which define a group of N_{tri} TCPEs. A minimum number of four markers is needed to have more than one TCPE in a cluster. The non-rigid kinematics of each TCPE is presented here.

A. Kinematics of a TCPE

The present configuration of a given TCPE at time t is characterized by the position vectors

$\{\boldsymbol{x}_1, \boldsymbol{x}_2, \boldsymbol{x}_3\}$ of the three vertices of the TCPE, relative to a fixed (inertial) point. The values of the position vectors in the reference configuration are denoted by the vectors $\{\boldsymbol{X}_1, \boldsymbol{X}_2, \boldsymbol{X}_3\}$ with $\boldsymbol{X}_i = \boldsymbol{x}_i(t = t_0)$; $i = 1,2,3$ where $t = t_0$ is an arbitrary fixed time.

The present and reference configurations are characterized by the director vectors $\{\boldsymbol{d}_1, \boldsymbol{d}_2, \boldsymbol{d}_3\}$ and $\{\boldsymbol{D}_1, \boldsymbol{D}_2, \boldsymbol{D}_3\}$, respectively, with $\boldsymbol{D}_3$ and $\boldsymbol{d}_3$ being normal to the plane of the TCPE, as shown in Fig. 1.

$$\begin{aligned}
&\boldsymbol{d}_1 = \boldsymbol{x}_2 - \boldsymbol{x}_1,\ \boldsymbol{d}_2 = \boldsymbol{x}_3 - \boldsymbol{x}_1,\ \boldsymbol{d}_3 = \frac{\boldsymbol{d}_1 \times \boldsymbol{d}_2}{|\boldsymbol{d}_1 \times \boldsymbol{d}_2|} \\
&\boldsymbol{D}_i = \boldsymbol{d}_i(t = t_0)\ ;\ i = 1,2,3 \\
&D^{1/2} = \boldsymbol{D}_1 \times \boldsymbol{D}_2 \cdot \boldsymbol{D}_3 > 0,\ A = \frac{1}{2} D^{1/2}
\end{aligned} \tag{1}$$

where A is the TCPE's reference area. Then, the reference reciprocal vectors $\{\boldsymbol{D}^1, \boldsymbol{D}^2, \boldsymbol{D}^3\}$ are defined by

$$\begin{aligned}
&\boldsymbol{D}^1 = D^{-1/2}(\boldsymbol{D}_2 \times \boldsymbol{D}_3) \\
&\boldsymbol{D}^2 = D^{-1/2}(\boldsymbol{D}_3 \times \boldsymbol{D}_1) \\
&\boldsymbol{D}^3 = D^{-1/2}(\boldsymbol{D}_1 \times \boldsymbol{D}_2) = \boldsymbol{D}_3 \\
&\boldsymbol{D}^i \cdot \boldsymbol{D}_j = \delta^i_j
\end{aligned} \tag{2}$$

where δ^i_j is the Kronecker delta symbol. Furthermore, the deformation gradient tensor $\boldsymbol{F}$ of the TCPE is defined using the tensor product (outer product) operator $\otimes$ in the expression

$$\boldsymbol{F} = \boldsymbol{d}_i \otimes \boldsymbol{D}^i \tag{3}$$

By definition, $\boldsymbol{F}$ is a nonsingular second order tensor so that the polar decomposition theorem [27] is used to determine its unique proper orthogonal rotation tensor $\boldsymbol{R}$ and the unique positive definite symmetric stretch tensor $\boldsymbol{M}$. Moreover, the Lagrangian strain tensor $\boldsymbol{E}$ of the TCPE is defined by

$$\begin{aligned}
&\boldsymbol{F} = \boldsymbol{R}\boldsymbol{M}\ ;\ [\boldsymbol{R}^T\boldsymbol{R} = \boldsymbol{I},\ \det(\boldsymbol{R}) = 1,\ \boldsymbol{M}^T = \boldsymbol{M}] \\
&\boldsymbol{R} = \boldsymbol{F}\boldsymbol{M}^{-1} = \boldsymbol{F}\left(\boldsymbol{F}^T\boldsymbol{F}\right)^{-1/2} ;\ \boldsymbol{E} = \frac{1}{2}\left(\boldsymbol{F}^T\boldsymbol{F} - \boldsymbol{I}\right)
\end{aligned} \tag{4}$$

More details regarding the computation of $\boldsymbol{M}$ are given in Appendix 1. Moreover, the difference between $\boldsymbol{R}$ and the rotation tensor obtained by applying the PS approach on the same cluster is discussed in Appendix 2.

Furthermore, the centroids of the TCPE $\{\bar{\boldsymbol{X}}, \bar{\boldsymbol{x}}\}$ in its reference and present configurations respectively, are given by

$$\bar{\boldsymbol{X}} = \frac{1}{3}\left(\boldsymbol{X}_1 + \boldsymbol{X}_2 + \boldsymbol{X}_3\right),\ \ \bar{\boldsymbol{x}} = \frac{1}{3}\left(\boldsymbol{x}_1 + \boldsymbol{x}_2 + \boldsymbol{x}_3\right) \tag{5}$$

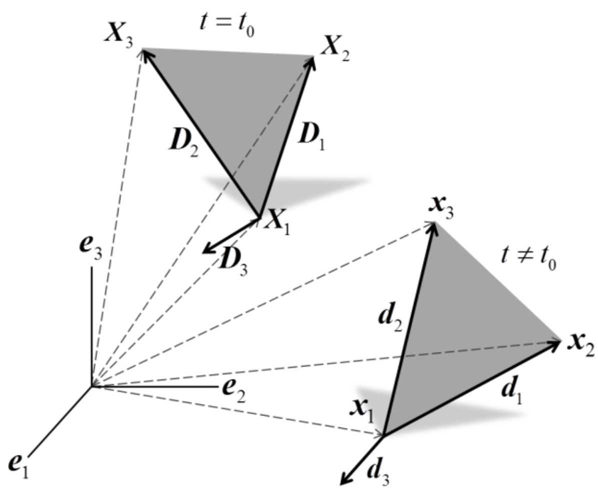

Fig. 1. Positions of a TCPE in its reference (t_0) and present (t) configurations with $\boldsymbol{D}_3$ and $\boldsymbol{d}_3$ being normal to the plane of the TCPE.

Let $\boldsymbol{X}^{(B)}$ be the position vector of the point B fixed to the relevant bone segment in the reference configuration, and $\boldsymbol{x}^{(B)}$ its position in the present configuration. Then, assuming that B is a material point of a body experiencing the homogeneous deformation of the TCPE, the position $\boldsymbol{x}_i$ of the node of a generic TCPE in the present configuration can be described by

$$\boldsymbol{x}_i = \boldsymbol{x}^{(B)} + \boldsymbol{F}\left(\boldsymbol{X}_i - \boldsymbol{X}^{(B)}\right);\ i = 1,2,3 \tag{6}$$

Thus, the translation vector $\boldsymbol{t}^{(B)}$ of point B from its reference position to its present configuration can be determined in terms of the reference and current positions of the centroid of the TCPE

$$\boldsymbol{t}^{(B)} = \boldsymbol{x}^{(B)} - \boldsymbol{X}^{(B)} = \bar{\boldsymbol{x}} - \boldsymbol{F}\left(\bar{\boldsymbol{X}} - \boldsymbol{X}^{(B)}\right) - \boldsymbol{X}^{(B)} \tag{7}$$

B. Physical Scalar TCPE Parameters

For ideal rigid body motion, all TCPEs have the same rotation tensor $\boldsymbol{R}$, their strain tensors $\boldsymbol{E}$ vanish, and the translation vectors $\boldsymbol{t}^{(B)}$ estimated by each of them are identical. Conversely, when markers are placed on a deformable body, the non-zero strain tensor $\boldsymbol{E}_J$ of the J$^{\text{th}}$ TCPE can be used to compute the magnitude E_J of the strain in the J$^{\text{th}}$ TCPE at time t:

$$E_J = \sqrt{\boldsymbol{E}_J \bullet \boldsymbol{E}_J} \tag{8}$$

where $\boldsymbol{A} \bullet \boldsymbol{B} = tr(\boldsymbol{A}\boldsymbol{B}^T)$ is the inner product of two second order tensors $\{\boldsymbol{A}, \boldsymbol{B}\}$. In addition, at time *t*, pairs of TCPEs can rotate relative to each other and the positive relative angle $\phi_{J/K}$ between them can be defined using the rotation tensors $\boldsymbol{R}_J$ and $\boldsymbol{R}_K$ estimated by the J^th^ and K^th^ TCPEs, respectively:

$$\phi_{J/K} = \cos^{-1}\left[\frac{1}{2}\left(\boldsymbol{R}_J \bullet \boldsymbol{R}_K - 1\right)\right] \tag{9}$$

Moreover, the average rotational parameter ϕ_J of the J^th^ TCPE relative to all other TCPEs at time *t* is defined as:

$$\phi_J = \frac{1}{N_{tri} - 1} \sum_{K=1}^{N_{tri}} \phi_{J/K} \tag{10}$$

Similarly, the translational difference $T_{J/K}$ between the J^th^ and K^th^ TCPE is defined using the translation vectors $\boldsymbol{t}_J^{(B)}$ and $\boldsymbol{t}_K^{(B)}$:

$$T_{J/K} = \left|\boldsymbol{t}_J^{(B)} - \boldsymbol{t}_K^{(B)}\right| \tag{11}$$

and the average translational parameter T_J of the J^th^ TCPE relative to all other TCPEs at time *t* is defined as:

$$T_J = \frac{1}{N_{tri} - 1} \sum_{K=1}^{N_{tri}} T_{J/K} \tag{12}$$

The scalars ϕ_J and T_J vanish when the markers forming the TCPEs all move as material points of a homogeneously deforming continua (which can include both RM and NRM components), whereas the scalar E_J vanishes for rigid body motion of the J^th^ TCPE. Therefore, all three scalars $\{E_J, \phi_J, T_J\}$ vanish for rigid body motion which is, in fact, a special homogeneous deformation that occurs when $\boldsymbol{F}$ is an orthogonal rotation tensor. It is important to emphasize that all scalar TCPE parameters are determined using only the skin markers trajectories; therefore they can be obtained noninvasively.

C. Rigid body motion errors of each TCPE

Rigid body motion errors for the orientation $\Delta\theta_J$ and position Δt_J of the Jth TCPE at time t are defined by:

$$\Delta\theta_J = \cos^{-1}\left[\frac{1}{2}\left(\boldsymbol{R}_J \bullet \boldsymbol{R}_{True} - 1\right)\right] \; ; \; \Delta t_J = \left|\boldsymbol{t}_J^{(B)} - \boldsymbol{t}_{True}^{(B)}\right| \tag{13}$$

where $\boldsymbol{t}_{True}^{(B)}$ is the true translation vector of the reference point B and $\boldsymbol{R}_{True}$ is the true rotation tensor of the bone with respect to the fixed laboratory frame.

D. Experimental Evaluation

To evaluate the effectiveness of the proposed method, the following experimental setup and data analysis were used. Complete details of the experimental data and procedures were described in previous works [8, 14, 23]. In brief, data were obtained from three intact cadavers (S1, S2, S3). Steel pins equipped with four markers were inserted into their right pelvis, femur, and tibia. Twelve skin markers were placed along three antero-lateral aspects of the right thigh, as shown in Fig. 2. An anatomical calibration procedure was performed to define the anatomical coordinate systems of the pelvis, femur and tibia [12] necessary for the determination of the hip and knee joint angles. The specimens were placed in a supine position (which was set as the reference configuration) with their lower limbs initially extended; thereafter an operator flexed their right hip and knee to the largest possible range of motion and then extended them back to the reference posture at a relatively low speed. The procedure was carried out three times for each specimen. The reference point B was taken as the origin of the femoral coordinate system located midway between the femoral condyles [24]. $\boldsymbol{X}^{(B)}$ in (6) and (7) is its position in the reference configuration. At each time step, the true translation vector $\boldsymbol{t}_{True}^{(B)}$ and the true rotation tensor $\boldsymbol{R}_{True}$ of the femur with respect to the fixed laboratory frame were obtained from the trajectories of the femur pin markers.

The cluster of twelve skin markers was used to construct all possible combinations of three markers, resulting in 220 TCPEs. Triangles having one of the interior angles smaller than 10 degrees were excluded, in order to prevent occurences of inversion of the TCPEs which are not physically admissible. Consequently, the number of included TCPEs N_{tri} was reduced to 198, 203, and 193, for S1, S2 and S3, respectively. At each time step and for each Jth TCPE, the trajectories of the skin markers were used to obtain its translation vector $\boldsymbol{t}_J^{(B)}$, rotation tensor $\boldsymbol{R}_J$, and the scalar parameters E_J, ϕ_J, and T_J. Skin and pin marker trajectories were used to compute the position error Δt_J and orientation error $\Delta\theta_J$ for each J$^{\text{th}}$ TCPE at time *t*. The position and orientation errors were also calculated by applying the PS approach on the entire cluster of markers [32].

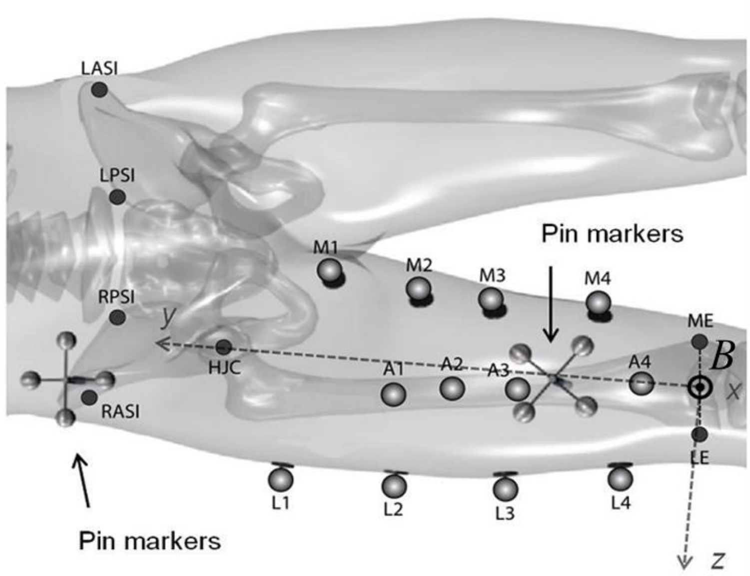

Fig. 2. Pin markers, skin markers L1-L4, A1-A4, M1-M4, anatomical landmarks calibrated on the pelvis and thigh segments, and reference point *B* at the origin of the femoral coordinate system.

E. Statistical Analysis

Shapiro-Wilk normality tests for each of the parameters $\{E_J, \phi_J, T_J, \Delta t_J, \Delta\theta_J\}$ indicated that none of them was normally distributed. Therefore, their dispersions over all TCPEs are described using the five-number summary technique (minimum, lower quartile, median, upper quartile, and maximum), and the data over all time steps and all trials are represented using box-plots.

To examine the relationship between the physical deformation parameters of each TCPE and the associated errors in the estimation of rigid body motion and to determine the feasibility to use these parameters to predict the accuracy of the TCPE pose estimation, Spearman's rank correlation coefficients (r_s) between the instantaneous errors $\Delta\theta_J$ and Δt_J and each of the instantaneous parameters $\{E_J, \phi_J, T_J\}$ were calculated at each time step. The values of r_s over all time steps and all trials are also represented using box-plots.

RESULTS

The median and interquartile (upper minus lower quartile, in brackets) values of the hip flexion-extension, hip abduction-adduction, hip internal-external rotation, and knee flexion-extension ranges recorded over all trials and specimens were 54.1 (20.5), 7.6 (1.8), 15.3 (7.1), and 101.8 (34.5) degrees, respectively.

Values of the parameters E_J, ϕ_J, and T_J for all TCPEs are shown as a function of time in Fig. 3a for a representative trial of each specimen. Statistics of these values, for all time steps and all trials, is presented in Fig. 3b. The median values for the three specimens ranged from 4.9 to 8.0% for E_J, from 5.7 to 7.5 degrees for ϕ_J, and from 14 to 16 mm for T_J. The maximum values recorded ranged from 37 to 61% for E_J, from 31 to 41 degrees for ϕ_J, and from 70 to 87 mm for T_J.

Values of the orientation errors $\Delta\theta_I$ and position errors Δt_I for all TCPEs are shown in Fig. 4a for the same representative trials as in Fig. 3a. The errors obtained by applying the PS approach [32] on the entire cluster of markers are plotted (dashed line) as a reference line for comparison. The knee flexion angles and the hip flexion, abduction, and external rotation angles are plotted for the same trials as well. Statistics of the pose errors, for all time steps and all trials, is presented in Fig. 4b.

The results indicate that subsets of all the TCPEs can estimate the underlying bone position and orientation considerably more accurately than the PS approach applied to the entire cluster of markers. Hypothetically, if the TCPEs which most accurately estimate the underlying bone position and orientation, could be identified at each time step, the root mean square errors would be reduced from 8.0 to 2.6 mm for position, and from 4.8 to 1.4 deg for orientation. Moreover, the number of TCPEs that exhibited errors smaller than those estimated by the PS approach applied to the entire cluster of markers was, on average, 21% for position errors and 31% for orientation errors.

Statistics of the values of the instantaneous Spearman correlation coefficients r_s between the TCPE parameters and the pose errors are presented in Fig. 5. Statistically, the pose errors were positively correlated with all three TCPE parameters. However, some parameters are better correlated than others. The strain parameter exhibited mostly poor to moderate correlations with the errors (median value of $\overline{r}_s = 0.40$ with the orientation error and $\overline{r}_s = 0.50$ with the position error), the rotational parameter exhibited strong correlation with the orientation error $\left(\overline{r}_s = 0.70\right)$ and moderate with the position error $\left(\overline{r}_s = 0.57\right)$, and the translational parameter exhibited strong correlation with the position error $\left(\overline{r}_s = 0.78\right)$ and moderate with the orientation error $\left(\overline{r}_s = 0.56\right)$.

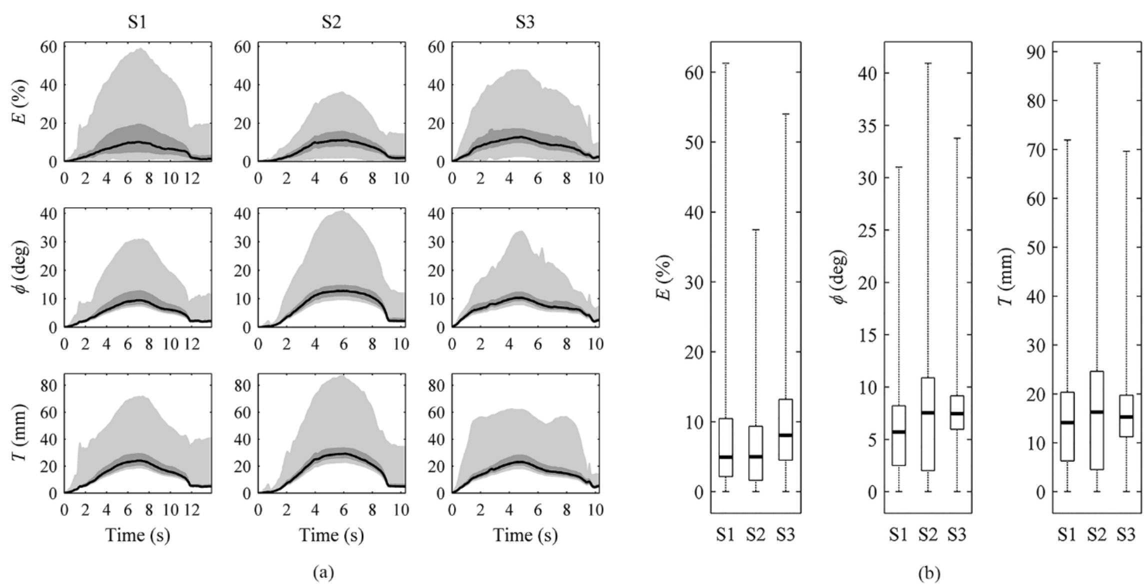

Fig. 3. Parameters E_I, ϕ_I, and T_I for all TCPEs. (a) The plots show, for a representative trial of each specimen (S1, S2, S3), the median (solid line), 25th-75th percentiles (dark grey band), and minimum-maximum range (light grey band). (b) The box-plots show the median, 25th-75th percentiles, and minimum-maximum ranges, recorded for all of the time steps during three trials per specimen.

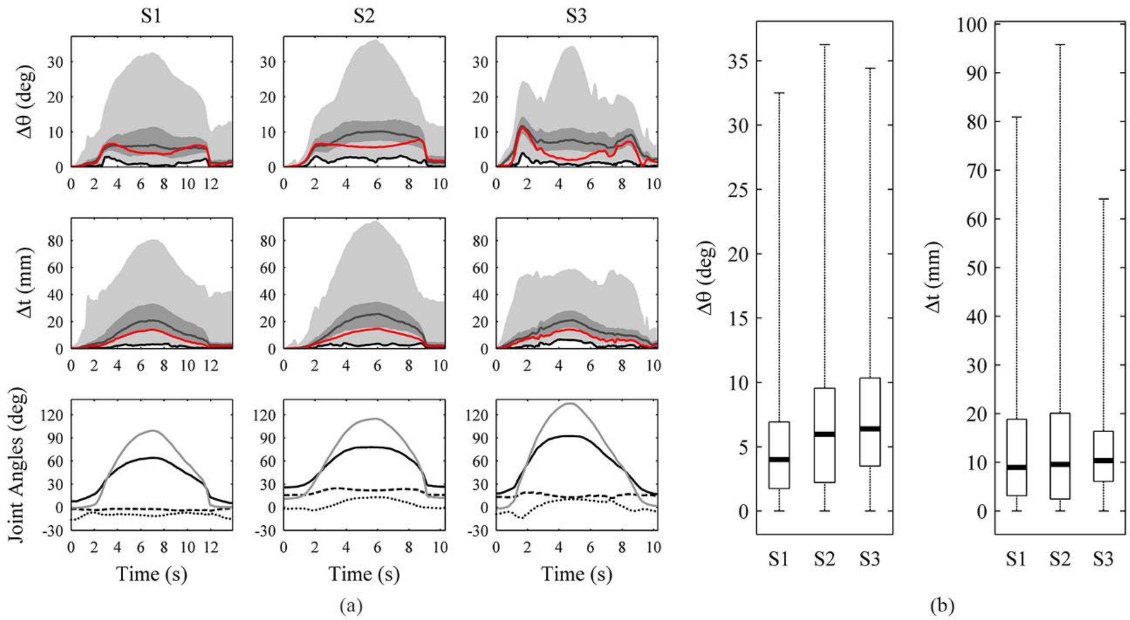

Fig. 4. Orientation errors $\Delta\theta_I$ and position errors Δt_I for all TCPEs. (a) The plots show, for a representative trial of each specimen (S1, S2, S3), the minimum (black line), median (dark grey line), 25th-75th percentiles (grey band), and range (light grey band). The errors obtained by applying the PS approach on the entire cluster of markers are plotted for comparison (red line). The lower panel shows the hip joint angles (flexion: solid black line, abduction: dashed line, external rotation: dotted line) and the knee flexion (grey line). (b) The box-plots show the median, 25th-75th percentiles, and minimum-maximum ranges of the errors, recorded for all of the time steps during three trials per specimen.

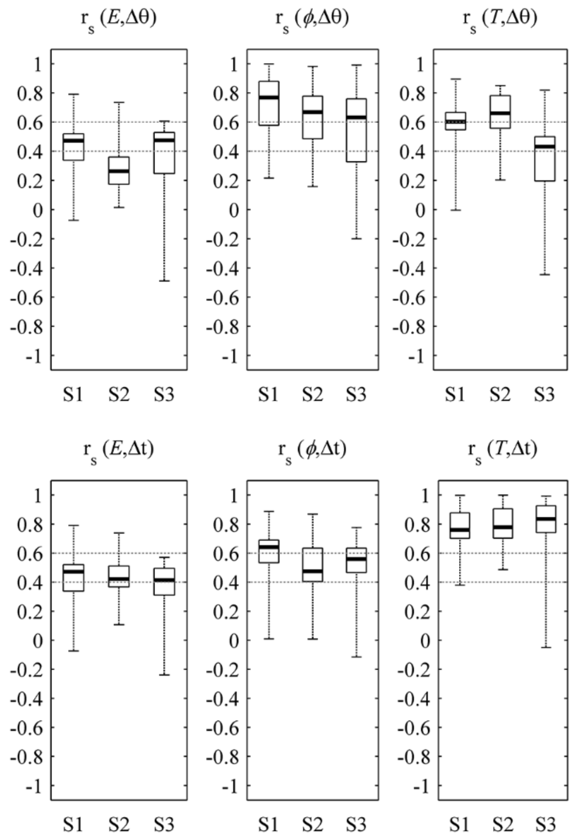

Fig. 5. Instantaneous Spearman correlation coefficients r_s between the parameters E_I, ϕ_I, and T_I, and the orientation errors $\Delta\theta_I$ and position errors Δt_I are presented. The box-plots show, for each specimen (S1, S2, S3), the median, 25^{th}-75^{th} percentiles, minimum and maximum, of r_s recorded for all TCPEs, time steps, and for all three trials of each specimen. The dotted reference lines represent moderate and strong correlations.

DISCUSSION

In the present study, the Triangular Cosserat Point Elements (TCPE) method, based on continuum mechanics, has been further developed for the bone pose estimation in the presence of the STA effects on a cluster of redundant skin markers. The kinematics of TCPEs obtained from all combinations of three markers was defined in terms of the deformation gradient tensors and the translation vectors between two configurations. Subsequently, three instantaneous physical scalar TCPE parameters were defined to characterize the magnitude of strain in each TCPE, and the relative rotation and relative translation between pairs of TCPEs. The possibility that these parameters correlate well with the accuracy of the bone pose estimated using specific TCPEs was tested using previously collected *ex-vivo* data, consisting of skin markers and bone pins, by investigating the relationship between the values of the TCPE parameters and the magnitudes of the position and orientation errors.

Analysis of the TCPE parameters revealed high variability across both TCPEs and specimens. The large non-rigidity of the cluster of markers is evident by the large values of strains recorded, as well as by the large relative rotation angles and relative translations between pairs of TCPEs. Nevertheless, examination of the position and orientation errors estimated by the different TCPEs indicates that, at each time step, there exist different subsets of TCPEs which represent the motion fairly accurately. It has been shown that, if the most accurate TCPEs could be identified at each time step, the pose errors would be reduced significantly compared with those obtained by the PS approach applied on the entire cluster of markers. This is an encouraging result because it confirms that there is no synchronous rigid motion of the entire marker set relative to the underlying bone [9], and that it may be possible to substantially reduce the STA propagation by identifying the TCPEs, at each time step, that best represent the bone pose, exhibiting the smaller orientation or position errors. It is important to note that TCPEs that exhibit small orientation errors can be different from those exhibiting small position errors. Moreover, these TCPEs can be different at different instants. Consequently, improvements in the bone pose estimation accuracy can be achieved by selecting different subsets of TCPEs at each instant for estimating the bone position and orientation.

The TCPEs which exhibit the most accurate pose estimations varied greatly across specimens and across time and included throughout the lower limb motion all twelve markers. Hence, with the present data set, it was impossible to suggest guidelines for the selection of specific optimal TCPEs or marker placements for the entire duration of all the trials. This finding justifies the instantaneous selection of subsets of TCPEs. Moreover, the fact that all twelve markers were necessary to compose the best instantaneous TCPEs justifies the use of a cluster containing a large number of markers.

The ability of the parameters to predict the accuracy of the TCPEs' bone pose estimation was evaluated by the instantaneous values of the correlation coefficients r_s between the parameters and the bone pose errors of the TCPEs. The results revealed mostly positive correlations between the three TCPE parameters and the position and orientation errors. The weakest correlations were found between the strain parameter E and the errors (mostly poor to moderate correlations), suggesting that the strain magnitude in a TCPE may not be the best parameter for selection of quality TCPEs to estimate bone pose. The strongest correlations were found between the rotational parameter ϕ and the orientation error and between the translational parameter T and the position error for all specimens. This suggests that at each instant, TCPEs with smaller ϕ are more likely to accurately represent the bone orientation and that TCPEs with smaller T are more likely to accurately represent the bone position. However, it was noted that the values of the correlation coefficients showed large variability over time, becoming poor in numerous instances. These findings seem to partially differ from those reported in previous studies [23, 35], that the NRM metrics for clusters of four markers were not markedly correlated with the pose errors. Nevertheless, these previous conclusions were based on inherently different metrics for the STA description than the TCPE parameters.

Moreover, it is important to stress that both ϕ_J and T_J are computed as average parameters and, therefore, they are influenced by the kinematic behavior of all other TCPEs which, in turn, depends on the number and locations of the markers. Low values of the rotational and translational parameters correspond to TCPEs which move in quasi-unison with the average motion of all TCPEs constructed from the twelve skin markers available. The strong correlations found between the rotational and translational parameters and the position and orientation errors also partially justify the use of a large number of markers for improving the bone pose estimation [15]. When accuracy is required, additional markers can be used since their placement depends only on technical requirements (i.e. marker inter-distance and visibility) and not on specific anatomical placement locations. Consequently, placement of these markers should not add considerable amount of time. Furthermore, it is worth noting that the proposed continuum model approach for the description of the skin markers' kinematic variables could also be applied to data recorded using markerless motion capture techniques. In the near future, markerless techniques will become more accessible and accurate [28, 31] and, in contrast with marker-based stereophotogrammetry, a very large number of observation points (a few hundreds per segment) will be available at minimal additional cost, either monetary or in subject preparation time [18].

The data used to examine the TCPE method here suffer from a number of limitations. Firstly, the STA measured in this study does not include all sources of the STA phenomenon, due to the lack of muscular activity and inertial effects normally associated with voluntary *in-vivo* motions. Nevertheless, previous work [7] has shown that for tasks not entailing abrupt accelerations, such as slow running, soft tissue wobbling and deformations due to muscle contraction and inertial effects (in non-obese subjects), have a smaller impact with respect to the STA associated with the passive joint movement. This suggests that the kinematic data used in this study exhibit comparable amplitudes to those observed in previous *in-vivo* studies [1, 6, 7, 13, 22, 36]. Secondly, the small number of specimens and the *ex-vivo* scenario prevent a generalization of the experimental results. However, the conceptual methods presented here remain valid.

In summary, the TCPE method proposes a number of physical parameters that can be used to describe, at each instant, the deformation of the body segment under analysis when the trajectories of several physical points of observation are available. It has been shown that some of these parameters correlate well with femur pose errors measured *ex-vivo*, which suggests that they can be used to select, at each instant, subsets of TCPEs which are more likely to accurately estimate the underlying bone pose. It has been shown that subsets of TCPEs exist which predict bone position and orientation more accurately than predicted by the PS approach applied on the entire cluster of markers, and that physical parameters of the TCPEs could be used as indicators to identify these subsets. It is expected that the operational framework provided by the TCPE method can be used to describe the body segment deformation and to lay the foundation for the compensation of the STA in *in-vivo* measurements of different populations, motor tasks and body segments when a high number of observation points are recorded. Future work will attempt to develop an advanced STA compensation procedure based on the TCPE parameters, using more comprehensive in-vivo data. This compensation procedure requires criteria for the instantaneous selection of subsets of TCPEs and an optimal technique for averaging the position and orientation of these subsets. Nevertheless, our preliminary analysis of the TCPE method in the presence of STA demonstrates its potential for improving the bone pose estimates with respect to those predicted using the entire cluster of markers.

APPENDIX 1

The objective of this appendix is to give more details regarding the computation of the kinematics of the TCPEs. The symmetric right Cauchy-Green deformation tensor $\boldsymbol{C}$ associated with the deformation gradient tensor $\boldsymbol{F}$ defined in (3) is used to calculate the stretch tensor $\boldsymbol{M}$, as follows:

$$\begin{aligned} &\boldsymbol{C} = \boldsymbol{F}^T \boldsymbol{F} \Rightarrow \boldsymbol{C} = \left(\boldsymbol{RM}\right)^T \boldsymbol{RM} = \boldsymbol{M}^T \boldsymbol{R}^T \boldsymbol{RM} = \boldsymbol{M}^T \boldsymbol{M} \\ &\Rightarrow \boldsymbol{M} = \boldsymbol{C}^{1/2} = \left(\boldsymbol{F}^T \boldsymbol{F}\right)^{1/2} \end{aligned} \tag{14}$$

APPENDIX 2

The objective of this appendix is to compare the rotation matrix of a cluster containing three markers obtained by the TCPE method with that obtained by the PS approach. Let $\{\boldsymbol{X}_0, \boldsymbol{X}_1, \boldsymbol{X}_2\}$ and $\{\boldsymbol{x}_0, \boldsymbol{x}_1, \boldsymbol{x}_2\}$ be the position vectors of three markers in the reference frame and in the present frame, respectively. In order to determine a 3×3 rotation matrix $\boldsymbol{Q}$ and a translation 3×1 vector $\boldsymbol{t}$ that map the points $\boldsymbol{X}_i$ to $\boldsymbol{x}_i$, the following least-squares problem is solved:

$$\min \sum_{i=1}^{3} \left\| \boldsymbol{Q}\boldsymbol{X}_i + \boldsymbol{t} - \boldsymbol{x}_i \right\|^2 \tag{15}$$

where $\boldsymbol{Q}$ is constrained to be an orthogonal rotation matrix that possess the properties

$$\boldsymbol{Q}^T \boldsymbol{Q} = \boldsymbol{I}\ , \quad \det(\boldsymbol{Q}) = 1 \tag{16}$$

The centroids $\{\bar{\boldsymbol{X}}, \bar{\boldsymbol{x}}\}$ introduced in (5) are used to define the vectors $\{\Delta\boldsymbol{X}_i, \Delta\boldsymbol{x}_i\}$ and the tensor $\bar{\boldsymbol{F}}$ by

$$\begin{aligned} &\Delta\boldsymbol{X}_i = \boldsymbol{X}_i - \bar{\boldsymbol{X}}\, ; \Delta\boldsymbol{x}_i = \boldsymbol{x}_i - \bar{\boldsymbol{x}} \\ &\bar{\boldsymbol{F}} = \Delta\boldsymbol{x}_i \otimes \Delta\boldsymbol{X}_i \end{aligned} \tag{17}$$

Then, the positive polar decomposition theorem can be used to decompose $\bar{\boldsymbol{F}}$ into its rotation tensor $\bar{\boldsymbol{R}}$ and stretch tensor $\bar{\boldsymbol{M}}$ which is a positive-definite symmetric tensor

$$\bar{\boldsymbol{F}} = \bar{\boldsymbol{R}}\bar{\boldsymbol{M}} \tag{18}$$

Different PS methods used for pose estimation [32, 34, 37] demonstrated that the rotation matrix $\boldsymbol{Q}$ which satisfies (15) under the constraint condition in (16) is

$$\boldsymbol{Q} = \bar{\boldsymbol{R}} \tag{19}$$

The PS methods mentioned above predict the same rotation tensor $\bar{\boldsymbol{R}}$ and differ only by their algorithms for deriving it, as demonstrated on Appendix 3. On the other hand, the deformation gradient tensor $\boldsymbol{F}$ defined by the TCPE method in (3) predicts the rotation tensor $\boldsymbol{R}$. In this regard, it is noted that $\boldsymbol{F}$ transforms any material line in the analyzed triangular body from the reference to the present configuration so that

$$\Delta\boldsymbol{x}_i = \boldsymbol{F}\Delta\boldsymbol{X}_i \tag{20}$$

Then, with the help of (4), (17), (18), and (20) it follows that

$$\bar{\boldsymbol{F}} = \bar{\boldsymbol{R}}\bar{\boldsymbol{M}} = \boldsymbol{F}\bar{\boldsymbol{H}} = \boldsymbol{R}\boldsymbol{M}\bar{\boldsymbol{H}}\,;\bar{\boldsymbol{H}} = \Delta\boldsymbol{X}_i \otimes \Delta\boldsymbol{X}_i, \tag{21}$$

In general, $\boldsymbol{M}$ does not commute with $\bar{\boldsymbol{H}}$, which proves that $\bar{\boldsymbol{R}}$ does not equal to $\boldsymbol{R}$ whenever $\boldsymbol{M}\bar{\boldsymbol{H}}$ is not a symmetric tensor. Moreover, it is noted that since the rotation obtained by the PS approach is used in several other methods [5, 9, 23] for defining different metrics for defining the STA components, these definitions are also affected by the differ rotation tensor obtained by the PS method and the TCPE method.

APPENDIX 3

The objective of this appendix is to demonstrate that the rotation matrices obtained by eigenvalue decomposition [34], polar decomposition [37] and singular value decomposition [32] are identical. The polar decomposition of the tensor $\bar{\boldsymbol{F}}$ defined in (17) can be used to obtain $\bar{\boldsymbol{R}}$ by

$$\begin{aligned}&\bar{\boldsymbol{F}} = \bar{\boldsymbol{R}}\bar{\boldsymbol{M}}\,;\ \left[\bar{\boldsymbol{R}}^T\bar{\boldsymbol{R}} = \boldsymbol{I}\ ,\bar{\boldsymbol{M}} = \bar{\boldsymbol{M}}^T\right]\\&\bar{\boldsymbol{F}}^T\bar{\boldsymbol{F}} = \bar{\boldsymbol{M}}^T\bar{\boldsymbol{M}} \Rightarrow \bar{\boldsymbol{R}} = \bar{\boldsymbol{F}}(\bar{\boldsymbol{F}}^T\bar{\boldsymbol{F}})^{-1/2} = \bar{\boldsymbol{F}}\bar{\boldsymbol{M}}^{-1}\end{aligned} \tag{22}$$

Similarly, the singular value decomposition of $\bar{\boldsymbol{F}}$ can be used to obtain the same $\bar{\boldsymbol{R}}$:

$$\begin{aligned}&\bar{\boldsymbol{F}} = \boldsymbol{U}\boldsymbol{\Sigma}\boldsymbol{V}^T;\ \left[\boldsymbol{U}^T\boldsymbol{U} = \boldsymbol{V}^T\boldsymbol{V} = \boldsymbol{I}\ ,\boldsymbol{\Sigma} = diagonal\right]\\&\bar{\boldsymbol{F}}^T\bar{\boldsymbol{F}} = \boldsymbol{V}\boldsymbol{\Sigma}^2\boldsymbol{V}^T \Rightarrow \bar{\boldsymbol{M}} = \boldsymbol{V}\boldsymbol{\Sigma}\boldsymbol{V}^T \Rightarrow \bar{\boldsymbol{M}}^{-1} = \boldsymbol{V}\boldsymbol{\Sigma}^{-1}\boldsymbol{V}^T\\&\Rightarrow \bar{\boldsymbol{R}} = \boldsymbol{U}\boldsymbol{V}^T = \boldsymbol{U}\boldsymbol{\Sigma}\boldsymbol{V}^T\boldsymbol{V}\boldsymbol{\Sigma}^{-1}\boldsymbol{V}^T = \bar{\boldsymbol{F}}\bar{\boldsymbol{M}}^{-1}\end{aligned} \tag{23}$$

and the eigenvalue decomposition of $\bar{\boldsymbol{F}}^T\bar{\boldsymbol{F}}$ yields the same $\bar{\boldsymbol{R}}$:

$$\begin{aligned}&\bar{\boldsymbol{F}}^T\bar{\boldsymbol{F}} = \boldsymbol{V}\boldsymbol{\Sigma}^2\boldsymbol{V}^T\ ;\ \left[\boldsymbol{V}^T\boldsymbol{V} = \boldsymbol{I}\ ,\boldsymbol{\Sigma} = diagonal\right]\\&\bar{\boldsymbol{M}} = \boldsymbol{V}\boldsymbol{\Sigma}\boldsymbol{V}^T;\bar{\boldsymbol{F}} = \bar{\boldsymbol{R}}\boldsymbol{V}\boldsymbol{\Sigma}\boldsymbol{V}^T \Rightarrow \bar{\boldsymbol{R}} = \bar{\boldsymbol{F}}\boldsymbol{V}\boldsymbol{\Sigma}^{-1}\boldsymbol{V}^T = \bar{\boldsymbol{F}}\bar{\boldsymbol{M}}^{-1}\end{aligned} \tag{24}$$

It should be noted that even though the different methods provide identical rotation matrices analytically, they rely on different numerical algorithms and their sensitivity to errors are different. Therefore, they might result in different estimates if the markers are badly configured [32].

REFERENCES

1. Akbarshahi, M., A. G. Schache, J. W. Fernandez, R. Baker, S. Banks, and M. G. Pandy. Non-invasive assessment of soft-tissue artifact and its effect on knee joint kinematics during functional activity. J. Biomech. 43:1292, 2010.

2. Andersen, M. S., M. Damsgaard, J. Rasmussen, D. K. Ramsey, and D. L. Benoit. A linear soft tissue artefact model for human movement analysis: Proof of concept using in vivo data. Gait Posture 35:606-611, 2012.

3. Ball, K. A. and M. R. Pierrynowski. Modeling of the pliant surfaces of the thigh and leg during gait. Proceedings of SPIE- BiOS'98 International Biomedical Optics Symposium 3254:435-446, 1998.

4. Barré, A., J. Thiran, B. M. Jolles, N. Theumann, and K. Aminian. Soft tissue artifact assessment during treadmill walking in subjects with total knee arthroplasty. IEEE Transactions on Biomedical Engineering 60:3131-3140, 2013.

5. Benoit, D. L., M. Damsgaard, and M. S. Andersen. Surface marker cluster translation, rotation, scaling and deformation: Their contribution to soft tissue artefact and impact on knee joint kinematics. J. Biomech. , 2015.

6. Benoit, D. L., D. K. Ramsey, M. Lamontagne, L. Xu, P. Wretenberg, and P. Renström. Effect of skin movement artifact on knee kinematics during gait and cutting motions measured in vivo. Gait Posture 24:152-164, 2006.

7. Bonci, T., V. Camomilla, R. Dumas, L. Chèze, and A. Cappozzo. A soft tissue artefact model driven by proximal and distal joint kinematics. J. Biomech. 47:2354-2361, 2014.

8. Camomilla, V., A. Cereatti, L. Chèze, and A. Cappozzo. A hip joint kinematics driven model for the generation of realistic thigh soft tissue artefacts. J. Biomech. 46:625-630, 2013.

9. Camomilla, V., M. Donati, R. Stagni, and A. Cappozzo. Non-invasive assessment of superficial soft tissue local displacements during movement: a feasibility study. J. Biomech. 42:931-937, 2009.

10. Cappello, A., R. Stagni, S. Fantozzi, and A. Leardini. Soft tissue artifact compensation in knee kinematics by double anatomical landmark calibration: Performance of a novel method during selected motor tasks. IEEE Trans. Biomed. Eng. 52:992-998, 2005.

11. Cappozzo, A., A. Cappello, U. D. Croce, and F. Pensalfini. Surface-marker cluster design criteria for 3-D bone movement reconstruction. IEEE Transactions on Biomedical Engineering 44:1165-1174, 1997.

12. Cappozzo, A., F. Catani, U. Della Croce, and A. Leardini. Position and orientation in space of bones during movement: anatomical frame definition and determination. Clin. Biomech. 10:171-178, 1995.

13. Cappozzo, A., F. Catani, A. Leardini, M. Benedetti, and U. DellaCroce. Position and orientation in space of bones during movement: Experimental artefacts. Clin. Biomech. 11:90-100, 1996.

14. Cereatti, A., M. Donati, V. Camomilla, F. Margheritini, and A. Cappozzo. Hip joint centre location: An ex vivo study. J. Biomech. 42:818-823, 2009.

15. Cereatti, A., U. Della Croce, and A. Cappozzo. Reconstruction of skeletal movement using skin markers: comparative assessment of bone pose estimators. J. Neuroeng Rehabil. 3:7, 2006.

16. Challis, J. H. A procedure for determining rigid body transformation parameters. J. Biomech. 28:733-737, 1995.

17. Cheze, L., B. Fregly, and J. Dimnet. A Solidification Procedure to Facilitate Kinematic Analyses Based on Video System Data. J. Biomech. 28:879-884, 1995.

18. Corazza, S., L. Muendermann, A. Chaudhari, T. Demattio, C. Cobelli, and T. Andriacchi. A markerless motion capture system to study musculoskeletal biomechanics: Visual hull and simulated annealing approach. Ann. Biomed. Eng. 34:1019-1029, 2006.

19. de Rosario, H., A. Page, A. Besa, V. Mata, and E. Conejero. Kinematic description of soft tissue artifacts: quantifying rigid versus deformation components and their relation with bone motion. Med. Biol. Eng. Comput. 50:1173-1181, 2012.

20. Dumas, R., V. Camomilla, T. Bonci, L. Cheze, and A. Cappozzo. Generalized mathematical representation of the soft tissue artefact. J. Biomech. 47:476-481, 2014.

21. Dumas, R., V. Camomilla, T. Bonci, L. Chèze, and A. Cappozzo. What Portion of the Soft Tissue Artefact Requires Compensation When Estimating Joint Kinematics? Journal of Biomechanical Engineering 137:064502-064502, 2015.

22. Gao, B. and N. Zheng. Investigation of soft tissue movement during level walking: Translations and rotations of skin markers. J. Biomech. 41:3189-3195, 2008.

23. Grimpampi, E., V. Camomilla, A. Cereatti, P. De Leva, and A. Cappozzo. Metrics for describing soft-tissue artefact and its effect on pose, size, and shape of marker clusters. IEEE Transactions on Biomedical Engineering 61:362-367, 2014.

24. Grood, E. S. and W. J. Suntay. A joint coordinate system for the clinical description of three-dimensional motions: application to the knee. J. Biomech. Eng. 105:136, 1983.

25. Heller, M. O., S. Kratzenstein, R. M. Ehrig, G. Wassilew, G. N. Duda, and W. R. Taylor. The weighted optimal common shape technique improves identification of the hip joint center of rotation in vivo. Journal of Orthopaedic Research 29:1470-1475, 2011.

26. Leardini, A., L. Chiari, U. Della Croce, and A. Cappozzo. Human movement analysis using stereophotogrammetry - Part 3. Soft tissue artifact assessment and compensation. Gait Posture 21:212-225, 2005.

27. Malvern, L. E. Introduction to the mechanics of a continuous medium. : Prentice Hall, 1969.

28. Mündermann, L., S. Corazza, and T. P. Andriacchi. The evolution of methods for the capture of human movement leading to markerless motion capture for biomechanical applications. Journal of NeuroEngineering and Rehabilitation 3:6, 2006.

29. Peters, A., B. Galna, M. Sangeux, M. Morris, and R. Baker. Quantification of soft tissue artifact in lower limb human motion analysis: A systematic review. Gait Posture 31:1-8, 2010.

30. Rubin, M. Cosserat Theories: Shells, Rods and Points. : Kluwer, The Netherlands, 2000.

31. Schmitz, A., M. Ye, R. Shapiro, R. Yang, and B. Noehren. Accuracy and repeatability of joint angles measured using a single camera markerless motion capture system. J. Biomech. 47:587-591, 2014.

32. Söderkvist, I. and P. Wedin. Determining the movements of the skeleton using well-configured markers. J. Biomech. 26:1473-1477, 1993.

33. Solav, D., M. Rubin, and A. Wolf. Soft Tissue Artifact compensation using Triangular Cosserat Point Elements (TCPEs). Int. J. Eng. Sci. 85:1-9, 2014.

34. Spoor, C. W. and F. E. Veldpaus. Rigid body motion calculated from spatial co-ordinates of markers. J. Biomech. 13:391-393, 1980.

35. Stagni, R. and S. Fantozzi. Can cluster deformation be an indicator of soft tissue artefact? Gait Posture 30:S55, 2009.

36. Stagni, R., S. Fantozzi, A. Cappello, and A. Leardini. Quantification of soft tissue artefact in motion analysis by combining 3D fluoroscopy and stereophotogrammetry: a study on two subjects. Clin. Biomech. 20:320-329, 2005.

37. Veldpaus, F. E., H. J. Woltring, and L. J. M. G. Dortmans. A least-squares algorithm for the equiform transformation from spatial marker co-ordinates. J. Biomech. 21:45-54, 1988.